Published in final edited form as:
Cancer Prev Res (Phila). 2012 November ; 5(11): 1280–1290. doi:10.1158/1940-6207.CAPR-12-0132.

Multiphoton tomographic imaging: a potential optical biopsy tool for detecting gastrointestinal inflammation and neoplasia

Tomoki Makino[1,3,*], **Manu Jain**[2,5,*], **David C. Montrose**[1,*], **Amit Aggarwal**[2], **Joshua Sterling**[2], **Brian P. Bosworth**[1], **Jeffrey W. Milsom**[3], **Brian D. Robinson**[4], **Maria M. Shevchuk**[4], **Kathy Kawaguchi**[4], **Ning Zhang**[1], **Christopher M. Brown**[7], **David R. Rivera**[7], **Wendy O. Williams**[8], **Chris Xu**[7], **Andrew J. Dannenberg**[1,6], and **Sushmita Mukherjee**[2,6]

[1]Department of Medicine, Weill Medical College of Cornell University, New York, New York

[2]Department of Biochemistry, Weill Medical College of Cornell University, New York, New York

[3]Department of Surgery, Weill Medical College of Cornell University, New York, New York

[4]Department of Pathology and Laboratory Medicine, Weill Medical College of Cornell University, New York, New York

[5]Department of Urology, Weill Medical College of Cornell University, New York, New York

[6]Weill Cornell Cancer Center, Weill Medical College of Cornell University, New York, New York

[7]School of Applied and Engineering Physics, Cornell University, Ithaca

[8]Center for Animal Resources and Education, Cornell University, Ithaca

Abstract

Endoscopy is widely used to detect and remove premalignant lesions with the goal of preventing gastrointestinal (GI) cancers. Because current endoscopes do not provide cellular resolution, all suspicious lesions are biopsied and subjected to histological evaluation. Technologies that facilitate directed biopsies should decrease both procedure-related morbidity and cost. Here we explore the use of multiphoton microscopy (MPM), an optical biopsy tool that relies on intrinsic tissue emissions, to evaluate pathology in both experimental and human GI specimens, using hematoxylin and eosin (H&E)-stained sections from these tissues for comparison. After evaluating the entire normal mouse GI tract, MPM was used to investigate disease progression in mouse models of colitis and colorectal carcinogenesis. MPM provided sufficient histological detail to identify all relevant substructures in *ex vivo* normal GI tissue, visualize both acute and resolving stages of colitis, and show the progression of colorectal carcinogenesis. Next, *ex vivo* specimens from human subjects with celiac sprue, inflammatory bowel disease, and colorectal neoplasia were imaged by MPM. Finally, colonic mucosa in live anesthetized rats was imaged *in vivo* using a flexible endoscope prototype. In both animal models and human specimens, MPM images demonstrated a striking similarity to the results of H&E staining, as demonstrated by the 100% concordance achieved by the study pathologists' diagnoses. In summary, MPM is a promising technique that accurately visualizes histology in fresh, unstained tissues. Our findings support the continued development of MPM as a technology to enhance the early detection of GI pathologies including premalignant lesions.

Requests for reprint: Sushmita Mukherjee, PhD, MS, Department of Biochemistry, Room E 019A, Weill Medical College of Cornell University 1300 York Ave., New York, NY 10065, USA. Phone: 212-746-6495; Fax: 212-746-8875; smukherj@med.cornell.edu.

[*]These authors contributed equally to the study.

Disclosure of Potential Conflicts of Interest

No potential conflicts of interest were disclosed by the authors.

Introduction

Colorectal cancer (CRC) is the second leading cause of cancer-related deaths in the U.S with an estimated 140,000 new cases in 2011 (1). The use of colonoscopy to identify and remove premalignant colorectal adenomas reduces the risk of developing CRC (2). For average-risk individuals, colonoscopic screening is recommended every 10 years, beginning at age 50 (3). In individuals with a family history of CRC, earlier screening is recommended (3). Additionally, individuals with inflammatory bowel disease (IBD) for more than 8 years are at increased risk for developing CRC and surveillance colonoscopies including multiple random biopsies are recommended every 1–2 years (4, 5). Upon discovering dysplasia in an IBD patient, colectomy is often advised to prevent potential life-threatening CRC (6). Other gastrointestinal (GI) diseases that increase the risk of malignancy include Barrett's esophagus, chronic gastritis and celiac sprue (7–9). Improved imaging methods are needed for the early detection of premalignancy in both the upper and lower GI tract.

Current endoscopes, even with adjuncts to white light, i.e., pre- or post-processing image modulation or chromoendoscopy, do not provide cellular resolution that permit routine distinction between benign and dysplastic lesions. Consequently, the focus of endoscopic screening today is to biopsy or resect any suspicious lesions. The problems associated with such an approach include sampling error, removal of benign lesions, prolonged procedure times and multiple negative samples for pathologic interpretation leading to additional cost. Therefore, improved early detection methods which can facilitate targeted biopsies are needed.

Novel "optical biopsy" techniques, such as confocal microendoscopy and optical coherence tomography (OCT), can provide high-resolution imaging *in situ*, but each approach has significant limitations (10, 11). Here we explore the use of multiphoton microscopy (MPM) as a next-generation optical biopsy tool. MPM relies on the simultaneous absorption of two or three low energy (near-infrared) photons to cause a nonlinear excitation equivalent to that created by a single photon of bluer light. Excitation only occurs where there is sufficient photon density, i.e., at the point of laser focus, providing intrinsic optical sectioning. Tissue penetration is greater than with standard confocal microscopy because absorption and scattering of the laser excitation is reduced at near-infrared wavelengths (12, 13). Most importantly, by utilizing two-photon excitation in the 700–800 nm range, MPM enables both *in vivo* and *ex vivo* imaging of fresh, unprocessed and unstained tissue *via* intrinsic tissue emissions, which includes both autofluorescence and Second Harmonic Generation (SHG) (12–14). MPM imaging, utilizing intrinsic tissue emissions, is capable of generating distinct optical signals from different tissue components that enable imaging of animal (13, 15, 16) and human (17–22) tissues at sub-micron resolution in 3 dimensions to a depth of up to 0.5 mm below the specimen surface. These imaging parameters enable real-time detailed visualization of cellular and subcellular changes that accompany the development of disease.

Recent studies of MPM in multiple organ sites including the GI tract underscore the potential utility of this technology (18, 23–30). Although MPM has been previously used to assess GI tissue architecture in both animal models and human biopsies (18, 23–32), we posit that the current study is the most comprehensive evaluation of MPM imaging of the GI tract, carried out in four phases: (i) generation of an MPM atlas of the entire normal mouse GI tract, including the hepatobiliary system and pancreas (ii) imaging disease progression in mouse models of colitis and colorectal neoplasia (iii) visualization of human tissues from subjects with celiac sprue, IBD and colorectal neoplasia and (iv) *in vivo* imaging of the normal rat colon.

Materials and Methods

Procurement of mouse tissues for generating the normal GI atlas

The esophagus, stomach, duodenum, ileum and colon were harvested from 8 week-old C57BL6/J male mice (The Jackson Laboratory). All tissues were flushed with ice-cold phosphate buffered saline (PBS), cut open longitudinally and immediately imaged by MPM. Organs of the hepatobiliary system and pancreas were harvested and immediately imaged. Following imaging, tissues were fixed in 10% formalin overnight then paraffin embedded, sectioned and stained with hematoxylin and eosin (H&E).

Dextran sodium sulfate (DSS)-induced colitis

For studies of acute inflammation, 8 week-old male C57BL6/J mice were administered 2% DSS (MP Biochemical) dissolved in drinking water for 1, 3 or 7 days (n=3/time point). For studies of chronic inflammation, mice were given 2% DSS for 7 days, followed by 7 or 14 days of plain drinking water (n=3/time point). A separate control group of mice was given plain drinking water for the indicated experimental periods (n=2/time point). This experimental design is depicted in Supplementary Figure S1A. All mice were maintained on 5053 rodent diet 20 (PMI Nutrition, Inc.). At the end of the experimental period, mice were sacrificed and colons harvested, flushed with ice-cold PBS, cut open longitudinally and immediately imaged by MPM. Following imaging, colons were fixed in 10% formalin overnight then Swiss-rolled and paraffin embedded, sectioned and stained with H&E.

Azoxymethane (AOM)-induced colorectal carcinogenesis

Male A/J mice were placed on AIN93G purified diet (Research Diets, Inc.) and given 6 weekly intraperitoneal injections of AOM (10 mg/kg; Sigma Aldrich) or 0.9% saline beginning at 5 weeks of age. One, 3 or 7 weeks after the last injection, mice were sacrificed and colons were harvested and treated as described above. Three mice from the AOM-injected group and 2 mice from the saline-injected group were imaged at each time point. The experimental design is shown in Supplementary Figure S1B. The animal studies were approved by the Institutional Animal Care and Use Committee at Weill Cornell Medical College.

Procurement and imaging of human samples

Biopsy specimens from subjects with celiac sprue, Crohn’s disease, ulcerative colitis and their respective normal controls were collected during endoscopy. Immediately after biopsy, samples were placed in PBS on ice then imaged by MPM within 1 hour. Adenoma and adenocarcinoma specimens were collected from patients who underwent colectomy. After removal, colons were bisected in surgical pathology then imaged by MPM within 1 hour. After MPM imaging, biopsy and colectomy specimens were formalin fixed, paraffin embedded, sectioned and stained by H&E. Stained slides were evaluated by the attending pathology staff at New York-Presbyterian Hospital/Weill Cornell Medical College and reported using the World Health Organization guidelines (33). The study was approved by the Weill Cornell Medical College Institutional Review Board and all subjects provided written informed consent for participation.

Multiphoton microscopy

Olympus FluoView FV1000MPE imaging system was used for all MPM imaging, except the colectomy specimens, for which a home-built MPM system, described in detail previously (17), was used. Each specimen was placed at the center of a glass-bottomed 35-mm dish or a glass slide, with the luminal surface facing up, hydrated with PBS and overlaid with a coverslip. The whole dish was then placed under the objective of the upright microscope for imaging. Specimens were imaged first at low magnification using a 4X/0.28NA dry objective, and then at high magnification using a 25x/1.05NA or a 20X/0.95NA water immersion objective. Specimens were excited using 780 nm light from a tunable femtosecond pulsed Ti-Sapphire laser (Mai Tai DeepSee™, Spectra-Physics, Newport Corporation). Three distinct intrinsic tissue emission signals were collected using photomultiplier tubes in non-descanned configuration: (i) SHG (360–400 nm, color coded red), a nonlinear scattering signal originating from tissue collagen (ii) short wavelength autofluorescence (420–490 nm, color coded green), originating in part from reduced nicotinamide adenine dinucleotide (NADH) and flavin adenine dinucleotide (FAD) in cells, and elastin in the connective tissue and (iii) long wavelength autofluorescence (550–650 nm, color coded blue), originating in part from lipofuscin in macrophages, and from mucin and bile. The signals in individual channels were collected as separate grayscale images, color-coded and merged to produce the final image. Minor adjustments of brightness and color balance were carried out using Adobe Photoshop CS4.

For *in vivo* imaging, a prototype assembled at Cornell University, Ithaca (34; Fig 6A) was used. Briefly, the device consists of a miniaturized cantilever fiber raster scanner and a 0.8 numerical aperture gradient index (GRIN) lens, which are packaged into waterproof stainless steel housing. The entire rigid length of the prototype is 4 cm, with an outer diameter of 3 mm. Beyond this 4 cm rigid length, the rest of the device is flexible. The system is able to obtain raster scanned 512 × 512 pixel images, with a field of view of 115 × 115 μm, at 4.1 frames per second. The lateral and axial resolutions are 0.8 and 10 μm, respectively, which are comparable to the state-of-the-art commercial bench-top systems. For *in vivo* imaging (35), we used adult male Sprague Dawley rats (Charles River Laboratories International), since they are significantly larger, and thus more appropriate for imaging with the human endoscope prototype as compared to mice. In order to perform imaging, rats were placed under isofluorane anesthesia and a laparotomy was performed using a standard ventral midline abdominal approach. The colon was exteriorized, a section was placed on a flat platform and a small incision was made to expose the colonic mucosa and allow for the insertion of the endoscope. The colonic mucosa was visualized using femtosecond pulsed 800 nm light, and the endoscope was focused 20–30 μm below the mucosal surface (Fig 6B–C). The resultant emission was collected in two photomultiplier channels, one collecting SHG (≤405 nm) and another collecting broadband auto-fluorescence (≥405 nm). Images were acquired for several seconds at a time, and collected as movies. One of the frames of the movie was later extracted, color-coded green, and minimally processed (adjustment of brightness and contrast, and Gaussian smoothing to remove single pixel noise). In order to compare the performance of endoscopic imaging with that of the commercial bench-top Olympus FV1000MPE system, a section of colon was excised from an adult male Sprague Dawley rat after sacrifice, flushed with PBS, cut open longitudinally and imaged using the commercial system under comparable imaging parameters. This tissue was subsequently fixed in formalin, and processed for routine H&E histology, as described above.

Histopathological analysis

The three study pathologists first reviewed H&E-stained slides from the DSS and AOM models along with corresponding control tissues, to familiarize themselves with the morphological changes at various time points in the disease. Subsequently, each pathologist was independently shown representative MPM images of the same specimens in a blinded fashion. For the DSS model, each pathologist scored the morphological changes in the following categories: (a) crypt architecture (normal, atrophic, regenerative or dysplastic), (b) presence or absence of inflammation and (c) ulceration (n= 3 mice/group). Based on these morphological changes, each image was assigned either to the acute or the resolving phase of colitis. For the AOM model, pathologists were asked to identify the following lesions: (a) aberrant crypts, (b) aberrant crypt foci (ACF), (c) microadenoma and (d) adenoma (n= 3 mice/group). They also noted the degree of dysplasia (low or high) for each lesion.

For histopathological analysis of human specimens, MPM images of normal biopsies from the duodenum, terminal ileum and left colon were shown to two study pathologists. These locations were specifically chosen as controls for the diseased specimens which came from these parts of the GI tract. The pathologists were then shown MPM images from the suspected abnormal lesions in a blinded fashion, and asked to categorize them as lesions of malabsorption syndrome (celiac sprue) or IBD. These results were then compared with the diagnosis given on H&E-stained sections by the attending pathologists. The neoplastic lesions (adenomas and adenocarcinomas of the colon) were not included in the blinded analysis of MPM images since these images were generated from intact colectomy specimens and it could not be confirmed that H&E-stained slides used for clinical diagnosis were prepared from precisely the same locations as those imaged by MPM.

Results

MPM generates images of the mouse GI tract that are comparable to H&E-stained tissue

To determine whether MPM is useful for identifying pathology in the GI tract, we first created an atlas of the entire normal mouse GI tract, visualized by both MPM and concordant H&E staining. Beginning with the esophagus, Figure 1A–B shows typical morphology including keratinized stratified squamous epithelium lining the mucosa, as well as collagen bundles and elastin fibers within the submucosa. Next, the stomach was visualized showing gastric glands and connective tissue (Fig. 1C–D). Supplementary Figure S2A–D shows images of the gastroesophageal junction. The small intestine was next imaged including the duodenum and ileum which showed villi lined by enterocytes with interspersed goblet cells (Fig. 1E–H). MPM images of the ileum showed microvilli, which were only visible by MPM (Fig. 1G (inset)). Finally, we imaged the cecum and proximal colon which showed surface epithelium and crypts lined by columnar and goblet cells (Fig. 1I–L). Supplementary Figure S2E-H shows images of the ano-rectal junction. To complement these images of the tubular GI tract, the hepatobiliary system, including the gall bladder, liver, and pancreas were also imaged (Supplementary Fig. S3).

MPM can visualize stages of DSS-induced colonic injury

Studies were next undertaken to determine the utility of MPM to visualize colonic injury at different stages of experimental colitis. Colons from untreated mice had intact surface epithelium and normal appearing crypts (Fig. 2A–D). Neither MPM nor H&E revealed significant morphological changes after 1 or 3 days of DSS exposure. However, in mice given 7 days of DSS, we observed morphological changes associated with acute colitis including focal ulceration, atrophic crypts in areas of dropout, edema, and an inflammatory cell infiltrate in the lamina propria (Fig. 2E–H). Supplementary video SV1 highlights the 3-dimensional imaging capability of MPM which allows for better appreciation of histology in various tissue planes. Next, we visualized the resolving phase of colitis in mice administered DSS for 7 days followed by 7 days of plain drinking water (Fig. 2I–L). These images showed enlarged regenerative crypts within the mucosa and increased mononuclear inflammatory infiltrate in the lamina propria (Fig. 2I–L). Similar effects were seen 14 days after stopping DSS exposure.

The progression of colorectal carcinogenesis can be observed by MPM

To extend our preclinical studies of GI pathology, we next imaged the progression of experimental colorectal neoplasia in AOM-administered mice. Colons from saline-administered control mice had normal appearing crypt architecture and easily identifiable lymphoid follicles (Fig. 3A–D). By contrast, in AOM-administered mice, we observed aberrant crypt foci (ACF) comprised of hyperplastic and/or dysplastic crypts (Fig. 3E–H) as well as microadenomas, 1 week after the last of 6 weekly injections. Three weeks after the last AOM injection, a larger number of ACF with increasing degrees of dysplasia and more frequent microadenomas were found (Fig. 3I–L). At the final time point (7 weeks following the last injection), in addition to these early lesions, we also found macroadenomas lining the colonic mucosa with low and high-grade dysplasia (Fig. 3M–P).

Human GI disease can be visualized with MPM

We next determined whether our examination of GI pathology in mouse models could be translated to human disease. Therefore, we first examined endoscopic biopsies from small intestinal diseases that predispose to malignancy including celiac sprue and Crohn’s Disease. Duodenal biopsies from healthy subjects showed normal histology by MPM and H&E with villi lined by enterocytes and goblet cells (Fig. 4A–D). In contrast, duodenal biopsies from a celiac sprue subject revealed blunting of villi with flattened mucosal surface and lamina propria with increased lymphoplasmacytic infiltrate (Fig. 4E–H).

Next, we compared tissues from subjects with Crohn’s Disease *vs.* healthy controls. Figure 4I–L shows MPM and H&E images taken from the terminal ileum of a healthy subject showing normal histology. The biopsy taken from a subject previously diagnosed with Crohn’s disease however, showed features of chronic active ileitis with blunted villi and focal ulcerations containing inflammatory cells (Fig. 4M–P).

We extended our examination of human GI disease to visualize abnormalities of the colon. Figure 5 shows images of endoscopic biopsies from the colons of a healthy subject showing normal-appearing crypts (Fig. 5A–D) *vs.* clinically diagnosed chronic active ulcerative colitis (Fig. 5E–H). In the ulcerative colitis specimen, pseudopolyp formation, distortion and loss of crypts, and an inflammatory cell infiltrate are seen (Fig. 5E–H).

Finally, human colectomy specimens from subjects with colorectal neoplasia were imaged. Figure 5I–L shows a tubular adenoma with crowded glands lined by cells with elongated nuclei indicative of low-grade dysplasia. Figure 5M–P shows a well-differentiated adenocarcinoma with complex (back-to-back) arrangement of the tubular glands and cytological features of dysplasia. Taken together, the results obtained in both experimental models and humans indicate that MPM can be used to visualize GI diseases that predispose to cancer.

MPM-generated images allow for accurate pathological diagnoses

We next determined whether images generated by MPM alone could be used to identify and categorize GI diseases. H&E-stained sections from the same specimens imaged by MPM were used to confirm diagnoses. For mouse studies, colonic inflammatory lesions from mice exposed to DSS (n=3 mice/time point) were shown to three pathologists in a blinded fashion. Each viewer was able to identify normal, atrophic and regenerative crypts, and regions of ulceration and inflammation with 100% concordance with H&E-stained slides, as well as with 100% inter-observer agreement. Neoplastic lesions of the colon from AOM-exposed mice (n=3 mice/time point) were shown to pathologists to identify dysplastic crypts, ACF, microadenomas and macroadenomas in a blinded manner with 100% concordance. For both the DSS and AOM models, three pathologists were shown one low magnification image and three to six high magnification images generated by MPM. The low magnification images were tiles covering a relatively large area (10s of mm) in an effort to capture the heterogeneity of histological features seen at various stages of disease. High magnification images focused on structures of diagnostic importance.

For human samples, MPM images from clinically diagnosed subjects with Crohn's disease (n=4), ulcerative colitis (n=2) or celiac sprue (n=2) were examined by study pathologists. Images from IBD specimens (Crohn's disease or ulcerative colitis), were diagnosed as chronic active ileitis or chronic active colitis and samples from sprue cases were identified as such by MPM. These diagnoses were identical to the final pathology report given by attending pathologists based on H&E-stained slides prepared from the same specimens. As stated in the Methods section, neoplastic lesions from human samples were not included in the blinded analysis of MPM images since these images were generated from intact colectomy specimens and it could not be confirmed that H&E-stained slides used for clinical diagnosis were prepared from precisely the same locations as those imaged by MPM.

Imaging of colonic mucosa *in vivo* using a flexible MPM endoscope

We next assessed our ability to translate the *ex vivo* visualization of the animal and human GI tracts to *in vivo*. To this end, we utilized a miniaturized MPM endoscope prototype assembled at Cornell University, Ithaca (34, 35; Fig 6A–C). Imaging of the exposed colon in a live rat using this device showed all significant histological features including crypts lined by enterocytes and goblet cells (Fig. 6D). To compare the imaging capability of the prototype endoscope to the standard commercial bench-top system, excised rat colon tissue was also visualized using the bench-top microscope (Fig. 6E). Both systems showed striking similarity in their ability to reveal histological features (Fig. 6D–E). Standard H&E staining was also performed on the same tissue (Fig. 6F).

Discussion

The overall goal of this study was to assess the potential of MPM imaging for real-time high-resolution contrast-free visualization of both the normal GI tract and GI diseases linked to malignancy. To accomplish this, an MPM atlas of images of the entire normal mouse GI tract from the esophagus to the anus, including the organs of the hepatobiliary system and pancreas was generated. Next, mouse models of experimental colitis and colorectal neoplasia were imaged. MPM imaging was then used to visualize tissues from several diseases linked to GI malignancy including celiac sprue, IBD and colonic neoplasia. MPM images generated from tissues of both experimental models and human subjects recapitulated all essential aspects of histology found in H&E-stained sections. Finally, the feasibility of carrying out MPM imaging of the GI tract *in vivo* was established.

Previously, MPM imaging has been used to visualize the normal and diseased mouse GI tract (23, 24, 29, 30, 36). For example, DSS-induced colitis was imaged in green fluorescent protein transgenic mice (23, 24). Although these studies showed clear morphological changes in the colon as a result of DSS exposure, exogenous fluorescence was used to visualize these changes. Importantly, our study shows the ability of MPM to use endogenous tissue emission signals alone to image similar pathological changes. We posit that such imaging will be easier to translate to a clinical setting for future real-time endoscopic evaluation of tissue. Two-photon microscopy has also been used to show the aberrant morphology of a small intestinal polyp in $\mathrm{APC}^{\mathrm{Min}/+}$ mice (30). Our study builds upon this work and uses MPM to show the progression of morphological changes during colorectal carcinogenesis. One potential implication is that MPM-derived images may prove useful for determining the ability of chemopreventive agents to inhibit colorectal carcinogenesis.

After establishing the MPM signatures of colitis and colorectal neoplasia in the mouse model, we investigated whether similar changes could be identified in human disease. In each case, we found that MPM can reliably identify all relevant tissue substructures in the normal as well as the diseased human GI tract. Rogart et al. have utilized MPM to assess *ex vivo* specimens from several parts of the normal human GI mucosa identifying structures such as epithelial cells, goblet cells and interstitial fibers (18). Additionally, human esophageal, gastric and colon cancers have been previously investigated with MPM (18, 25, 26, 28, 30). To our knowledge, the current study provides the first evidence that MPM can be used to visualize and delineate morphological changes associated with celiac sprue, Crohn's ileitis and ulcerative colitis. Importantly, pathologists were able to use MPM to accurately diagnose each of these diseases that predispose to malignancy.

Confocal microendoscopy and OCT are two competing technologies for generating "optical biopsies" of diseased tissue. Endoscopes equipped with confocal imaging capabilities have been shown to be useful for detecting neoplastic changes in ulcerative colitis and Barrett's esophagus (37, 38). In another recent human study involving confocal microendoscopy, dysplastic colonocytes were shown to be preferentially labeled with a fluorescein-conjugated heptapeptide (39). However, in spite of the great promise, current clinical confocal systems suffer from several significant limitations including the need for exogenous contrast administration, shallow depth of imaging and only being able to detect the exogenously administered contrast agent. *In vivo* colonoscopic OCT has been used in clinical trials to distinguish between colonic polyps and normal mucosa and between ulcerative colitis and Crohn's disease (40, 41). The advantage of this technology is deeper tissue penetration (up to 2 mm) relative to both confocal and MPM, allowing access to the submucosa. However, the lateral resolution of current clinical systems (~10 micron) is insufficient to obtain the cellular and subcellular resolution that is necessary to distinguish between benign lesions and early stage neoplasms. Furthermore, unlike MPM, OCT does not generate distinct signals from specific tissue components. Thus, MPM imaging may overcome some of the limitations associated with confocal microendoscopy and OCT.

There are potential real-time clinical applications for MPM technology in human disease. In fact, a commercial MPM system (DermaInspect, JenLab) is currently approved in Europe for diagnosis of dermal neoplasms (42, 43). Furthermore, rigid microprobe objectives for use with bench-top MPM systems are commercially available but have only been used to image tissues *ex vivo* (18). Next generation technologies where MPM devices are miniaturized for use in rigid and flexible endoscopes, including the prototype used in this study, are currently under development in several laboratories (34, 44–50). Future uses for a rigid probe could include examination of the oral and vaginal mucosa and the anal/peri-anal region to identify dysplastic changes and exclude malignant lesions. Rigid probes could also be useful for evaluating surgical margins. Flexible endoscopes (similar to the one used in this study) could be utilized during colonoscopy and upper GI endoscopy to diagnose polyps and other suspicious regions within the mucosa as benign or malignant, thereby potentially minimizing biopsies of benign tissues. It is likely that using this technology will save time and reduce both patient morbidity and cost. Given the necessarily small field-of-view of any high-resolution optical biopsy technique, we visualize their role in the near future primarily as a means to confirm the identities of suspicious lesions found with low-resolution screening techniques, such as high-definition white light endoscopy, narrow band imaging or chromoendoscopy. In summary, our findings demonstrate the utility of MPM for imaging inflammatory and neoplastic lesions of the GI tract and support the continued development of MPM. Taken together, MPM may enhance the identification of GI pathology *in situ* during an endoscopic or surgical procedure, and thereby play a future role in preventing the development and progression of disease.

Supplementary Material

Refer to Web version on PubMed Central for supplementary material.

Acknowledgments

The authors acknowledge Dr. Parul Shukla, GI surgeon, for many useful discussions regarding the wider implications of MPM in surgical management of GI diseases, and Dr. Nicole Panarelli, GI pathologist, for review of some H&E slides which had ambiguous diagnoses.

Grant Support

This project was supported by the New York Crohn's Foundation (A. J. Dannenberg), The Uehara Memorial Foundation (T. Makino), NIH T32 CA062948 (D.C. Montrose) and NIH/NIBIB R01-EB006736 and NIH/NCI R01-CA133148 (C. Xu).

References

1. American Cancer Society. Cancer Facts and Figures 2011. Vol. 2011. Atlanta, GA: American Cancer Society; 2011.
2. Zauber AG, Winawer SJ, O'Brien MJ, Lansdorp-Vogelaar I, van Ballegooijen M, Hankey BF, et al. Colonoscopic polypectomy and long-term prevention of colorectal-cancer deaths. N Engl J Med. 2012; 366:687–96. [PubMed: 22356322]
3. Levin B, Lieberman DA, McFarland B, Andrews KS, Brooks D, Bond J, et al. Screening and surveillance for the early detection of colorectal cancer and adenomatous polyps, 2008: a joint guideline from the American Cancer Society, the US Multi-Society Task Force on Colorectal Cancer, and the American College of Radiology. Gastroenterology. 2008; 134:1570–95. [PubMed: 18384785]
4. Eaden JA, Mayberry JF, Gastroenterology BSf. Ireland AoCfGBa. Guidelines for screening and surveillance of asymptomatic colorectal cancer in patients with inflammatory bowel disease. Gut. 2002; 51 (Suppl 5):V10–2. [PubMed: 12221032]
5. Itzkowitz SH, Present DH. Group CsaCFoACCiIS. Consensus conference: Colorectal cancer screening and surveillance in inflammatory bowel disease. Inflamm Bowel Dis. 2005; 11:314–21. [PubMed: 15735438]
6. Mowat C, Cole A, Windsor A, Ahmad T, Arnott I, Driscoll R, et al. Guidelines for the management of inflammatory bowel disease in adults. Gut. 2011; 60:571–607. [PubMed: 21464096]
7. Prasad GA, Bansal A, Sharma P, Wang KK. Predictors of progression in Barrett's esophagus: current knowledge and future directions. Am J Gastroenterol. 2010; 105:1490–502. [PubMed: 20104216]
8. Howdle PD, Jalal PK, Holmes GK, Houlston RS. Primary small-bowel malignancy in the UK and its association with coeliac disease. QJM. 2003; 96:345–53. [PubMed: 12702783]
9. Catassi C, Bearzi I, Holmes GK. Association of celiac disease and intestinal lymphomas and other cancers. Gastroenterology. 2005; 128:S79–86. [PubMed: 15825131]
10. Paull PE, Hyatt BJ, Wassef W, Fischer AH. Confocal laser endomicroscopy: a primer for pathologists. Arch Pathol Lab Med. 2011; 135:1343–8. [PubMed: 21970490]
11. Thekkek N, Anandasabapathy S, Richards-Kortum R. Optical molecular imaging for detection of Barrett's-associated neoplasia. World J Gastroenterol. 2011; 17:53–62. [PubMed: 21218084]
12. Denk W, Strickler JH, Webb WW. Two-photon laser scanning fluorescence microscopy. Science. 1990; 248:73–6. [PubMed: 2321027]
13. Zipfel WR, Williams RM, Christie R, Nikitin AY, Hyman BT, Webb WW. Live tissue intrinsic emission microscopy using multiphoton-excited native fluorescence and second harmonic generation. Proc Natl Acad Sci U S A. 2003; 100:7075–80. [PubMed: 12756303]
14. Zipfel WR, Williams RM, Webb WW. Nonlinear magic: multiphoton microscopy in the biosciences. Nat Biotechnol. 2003; 21:1369–77. [PubMed: 14595365]

15. Ramasamy R, Sterling J, Fisher ES, Li PS, Jain M, Robinson BD, et al. Identification of spermatogenesis with multiphoton microscopy: an evaluation in a rodent model. J Urol. 2011; 186:2487–92. [PubMed: 22019169]
16. Ramasamy R, Sterling J, Li PS, Robinson BD, Parekattil S, Chen J, et al. Multiphoton Imaging and laser ablation of rodent spermatic cord nerves: potential treatment for patients with chronic orchialgia. Journal of Urology. 2012; 187:733–8. [PubMed: 22177201]
17. Mukherjee S, Wysock JS, Ng CK, Akhtar M, Perner S, Lee MM, et al. Human bladder cancer diagnosis using Multiphoton microscopy. Proc Soc Photo Opt Instrum Eng. 2009:7161.
18. Rogart JN, Nagata J, Loeser CS, Roorda RD, Aslanian H, Robert ME, et al. Multiphoton imaging can be used for microscopic examination of intact human gastrointestinal mucosa ex vivo. Clin Gastroenterol Hepatol. 2008; 6:95–101. [PubMed: 18065276]
19. Yadav R, Mukherjee S, Hermen M, Tan G, Maxfield FR, Webb WW, et al. Multiphoton microscopy of prostate and periprostatic neural tissue: a promising imaging technique for improving nerve-sparing prostatectomy. J Endourol. 2009; 23:861–7. [PubMed: 19425823]
20. Jain M, Robinson BD, Scherr DS, Sterling J, Lee M-M, Wysock J, et al. Multiphoton Microscopy in the Evaluation of Human Bladder Biopsies. Arch Pathol Lab Med. 2012; 136:517–26. [PubMed: 22540300]
21. Najari BB, Ramasamy R, Sterling J, Aggarwal A, Sheth S, Li PS, et al. Pilot study on the correlation of multiphoton tomography of *ex vivo* human testis with histology. Journal of Urology. 2012; 188:538–43. [PubMed: 22704107]
22. Tewari AK, Shevchuk MM, Sterling J, Grover S, Herman M, Yadav R, et al. Multiphoton microscopy for structure identification in human prostate and periprostatic tissue: implications in prostate cancer surgery. BJU Int. 2011; 108:1421–9. [PubMed: 21443651]
23. Morimoto Y, Tanaka K, Toiyama Y, Inoue Y, Araki T, Uchida K, et al. Intravital three-dimensional dynamic pathology of experimental colitis in living mice using two-photon laser scanning microscopy. J Gastrointest Surg. 2011; 15:1842–50. [PubMed: 21796457]
24. Toiyama Y, Mizoguchi A, Okugawa Y, Koike Y, Morimoto Y, Araki T, et al. Intravital imaging of DSS-induced cecal mucosal damage in GFP-transgenic mice using two-photon microscopy. J Gastroenterol. 2010; 45:544–53. [PubMed: 20058031]
25. Yan J, Chen G, Chen J, Liu N, Zhuo S, Yu H, et al. A pilot study of using multiphoton microscopy to diagnose gastric cancer. Surg Endosc. 2011; 25:1425–30. [PubMed: 21046158]
26. Chen J, Zhuo S, Chen G, Yan J, Yang H, Liu N, et al. Establishing diagnostic features for identifying the mucosa and submucosa of normal and cancerous gastric tissues by multiphoton microscopy. Gastrointest Endosc. 2011; 73:802–7. [PubMed: 21457819]
27. Liu N, Chen G, Chen J, Yan J, Zhuo S, Zheng L, et al. Multiphoton microscopic imaging of normal human rectum tissue. Scanning. 2010; 32:347–50. [PubMed: 20718013]
28. Zhuo S, Yan J, Chen G, Chen J, Liu Y, Lu J, et al. Label-free monitoring of colonic cancer progression using multiphoton microscopy. Biomed Opt Express. 2011; 2:615–9. [PubMed: 21412466]
29. Bao H, Boussioutas A, Reynolds J, Russell S, Gu M. Imaging of goblet cells as a marker for intestinal metaplasia of the stomach by one-photon and two-photon fluorescence endomicroscopy. J Biomed Opt. 2009; 14:064031. [PubMed: 20059269]
30. Grosberg LE, Radosevich AJ, Asfaha S, Wang TC, Hillman EM. Spectral characterization and unmixing of intrinsic contrast in intact normal and diseased gastric tissues using hyperspectral two-photon microscopy. PLoS One. 2011; 6:e19925. [PubMed: 21603623]
31. Tanaka K, Morimoto Y, Toiyama Y, Okugawa Y, Inoue Y, Uchida K, et al. Intravital dual-colored visualization of colorectal liver metastasis in living mice using two photon laser scanning microscopy. Microsc Res Tech. 2011
32. Ying M, Zhuo S, Chen G, Zhuo C, Lu J, Zhu W, et al. Real-time noninvasive optical diagnosis for colorectal cancer using multiphoton microscopy. Scanning. 2011
33. Bosman, FT.; Carneiro, F.; Hruban, RH.; Theise, ND. WHO Classification of Tumours of the Digestive System. 4. Geneva, Switzerland: World Health Organization; 2010.

34. Rivera DR, Brown CM, Ouzounov DG, Pavlova I, Kobat D, Webb WW, et al. Compact and flexible raster scanning multiphoton endoscope capable of imaging unstained tissue. Proc Natl Acad Sci U S A. 2011; 108:17598–603. [PubMed: 22006303]
35. Brown CM, Rivera DR, Ouzounov DG, Webb WW, Xu C. In vivo multiphoton endoscopy. J Biomed Optics. 2012; 17:040505.
36. Radosevich AJ, Bouchard MB, Burgess SA, Chen BR, Hillman EM. Hyperspectral in vivo two-photon microscopy of intrinsic contrast. Opt Lett. 2008; 33:2164–6. [PubMed: 18794965]
37. Goetz M, Kiesslich R. Confocal endomicroscopy: in vivo diagnosis of neoplastic lesions of the gastrointestinal tract. Anticancer Res. 2008; 28:353–60. [PubMed: 18383869]
38. Goetz M, Watson A, Kiesslich R. Confocal laser endomicroscopy in gastrointestinal diseases. J Biophotonics. 2011; 4:498–508. [PubMed: 21567975]
39. Hsiung PL, Hardy J, Friedland S, Soetikno R, Du CB, Wu AP, et al. Detection of colonic dysplasia in vivo using a targeted heptapeptide and confocal microendoscopy. Nat Med. 2008; 14:454–8. [PubMed: 18345013]
40. Shen B, Zuccaro G, Gramlich TL, Gladkova N, Trolli P, Kareta M, et al. In vivo colonoscopic optical coherence tomography for transmural inflammation in inflammatory bowel disease. Clin Gastroenterol Hepatol. 2004; 2:1080–7. [PubMed: 15625653]
41. Pfau PR, Sivak MV, Chak A, Kinnard M, Wong RC, Isenberg GA, et al. Criteria for the diagnosis of dysplasia by endoscopic optical coherence tomography. Gastrointest Endosc. 2003; 58:196–202. [PubMed: 12872085]
42. König K, Ehlers A, Riemann I, Schenkl S, Bückle R, Kaatz M. Clinical two-photon microendoscopy. Microsc Res Tech. 2007; 70:398–402. [PubMed: 17393493]
43. Paoli J, Smedh M, Ericson MB. Multiphoton laser scanning microscopy--a novel diagnostic method for superficial skin cancers. Semin Cutan Med Surg. 2009; 28:190–5. [PubMed: 19782943]
44. Chen M, Xu C, Webb WW. Endoscope lens with dual fields of view and resolutions for multiphoton imaging. Opt Lett. 2010; 35:2735–7. [PubMed: 20717440]
45. Liu G, Xie T, Tomov IV, Su J, Yu L, Zhang J, et al. Rotational multiphoton endoscopy with a 1 microm fiber laser system. Opt Lett. 2009; 34:2249–51. [PubMed: 19649060]
46. Bao H, Gu M. A 0.4-mm-diameter probe for nonlinear optical imaging. Opt Express. 2009; 17:10098–104. [PubMed: 19506662]
47. König K, Weinigel M, Hoppert D, Bückle R, Schubert H, Köhler MJ, et al. Multiphoton tissue imaging using high-NA microendoscopes and flexible scan heads for clinical studies and small animal research. J Biophotonics. 2008; 1:506–13. [PubMed: 19343676]
48. Rivera DR, Brown CM, Ouzounov DG, Webb WW, Xu C. Lensed fiber for a large field-of-view, high-resolution fiber-scanning microendoscope. Opt Lett. 2012; 37:881–3. [PubMed: 22378425]
49. Huland DM, Brown CM, Howard SS, Ouzounov DG, Pavlova I, Wang K, et al. *In vivo* imaging of unstained tissues using long gradient index lens multiphoton endoscopic systems. Biomedical Optics Express. 2012; 3:1077–85. [PubMed: 22567597]
50. Rivera DR, Brown CM, Ouzounov DR, Webb WW, Xu C. Multifocal multiphoton endoscope. Optics Letters. 2012; 37:1349–51. [PubMed: 22513682]

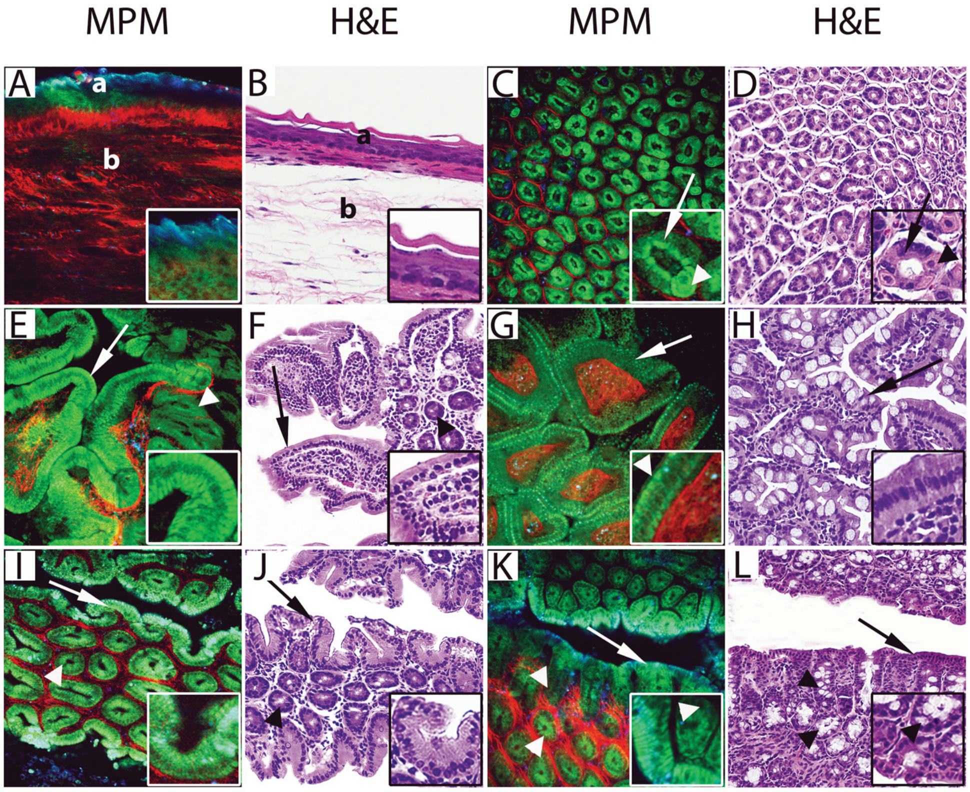

Figure 1.

Comparative MPM and H&E image atlas of the normal mouse gastrointestinal tract. A–B, The esophagus was imaged showing keratinized, stratified squamous epithelium lining the mucosa (a) and collagen bundles (red in MPM) and elastin fibers (green in MPM) in the submucosa (b). Insets in the MPM image show keratin (blue) and squamous cells (green). C–D, The stomach was imaged showing gastric glands (green in MPM) and the surrounding connective tissue (red in MPM). Insets show chief cells with basal nuclei (arrows) and large rounded parietal cells with central nuclei (arrowheads) lining a gastric gland. E–F, The duodenum was imaged showing villi (arrows) with core consisting of connective tissue (red in MPM) and mononuclear cells (mixture of blue and green cells in MPM) and crypts (arrowheads). Insets show enterocytes lining the villi. G–H, The ileum was imaged showing short and cylindrical villi (arrows) with the core consisting of connective tissue (red in MPM) and mononuclear cells (mixture of blue and green cells in MPM). Insets show enterocytes (green in MPM), microvilli (arrowhead in MPM) and connective tissue core (red in MPM). I–J, The cecum was imaged showing surface epithelium (arrows) and crypts of Lieberkühn (arrowheads). Insets show columnar epithelium of surface mucosa. K–L, The proximal colon was imaged showing surface epithelium (arrows) and crypts of Lieberkühn (arrowheads). Insets show surface epithelium and crypts lined by columnar epithelium and goblet cells (arrowheads).

(MPM total magnifications: A, C, E, G, I, K, = 300X, insets = 750X. H&E total magnifications: B, D, F, H, J, L, = 200X, insets = 400X).

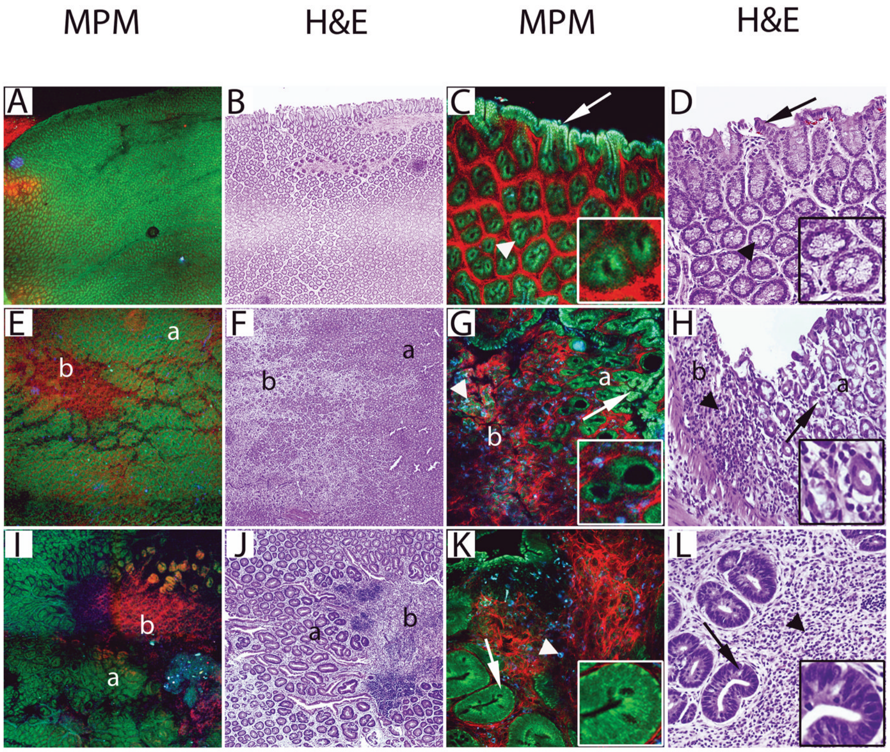

Figure 2.

MPM and H&E images of DSS-induced colonic injury. A–B, A control mouse colon was imaged showing colonic mucosa with uniform, homogenous crypts. C–D, High magnification images of panels A and B show columnar cells lining the surface epithelium (arrows), crypts (arrowheads and insets), and connective tissue (red in MPM) of the lamina propria. E–F, The colon from a mouse exposed to DSS for 7 days is shown at low magnification with a region of non-ulcerated colonic mucosa (a) and an ulcerated area with crypt loss and exposed connective tissue of the lamina propria (b). G–H, High magnification images of panels E and F show atrophic crypts (arrows and insets) in the non-ulcerated area (a) and exposed lamina propria with inflammatory cells (arrowheads) in the ulcerated area (b). I–J, A colon from a mouse given DSS for 7 days followed by 7 days of plain drinking water shows morphological features of resolving colitis at low magnification including a region with aberrant crypts (a) and an area of crypt loss associated with increased inflammatory cells and connective tissue (b). K–L, High magnification images show enlarged regenerative crypts (arrows and insets) from area ‘a’ in panels I and J and an increased number of mononuclear inflammatory cells (arrowheads) and connective tissue (red in MPM).

(MPM total magnifications: A, E, I = 48X, C, G, K = 300X, insets = 750X. H&E total magnifications: B, F, J = 40X, D, H, L = 200X, insets = 500X).

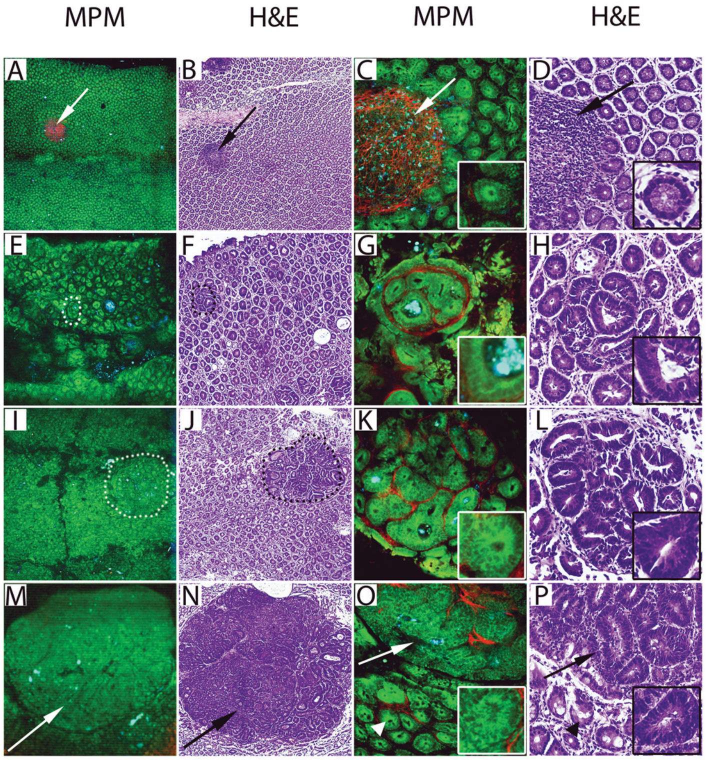

Figure 3.

Images of AOM-induced colonic neoplasia generated by MPM and H&E. A–D, Colonic mucosa from a saline-administered control mouse at low (A–B) and high (C–D) magnifications showing uniformly spaced homogenous crypts and a lymphoid follicle (arrows). Insets in panels C and D show a normal crypt at higher magnification. E–F, Images of an ACF are shown (dotted circle) on a background of polymorphic crypts within the colon one week following the last AOM injection. G–H, High magnification images of panels E and F show a well-defined ACF surrounded by a band of thick connective tissue (red in MPM). Insets show an ACF lined by cells with low-grade dysplasia defined by elongated and crowded nuclei. I–J, Images show a microadenoma three weeks following the last AOM injection (dotted circle), on a background of polymorphic appearing colonic mucosa. K–L, High magnification images of panels I and J show closely packed aberrant crypts with high-grade dysplasia defined by nuclear stratification and loss of goblet cells (insets) and little intervening connective tissue. M–N, Images show a macroadenoma (arrows) seven weeks following the last AOM injection. O–P, High magnification images of panels M and N show fused glands within the macroadenoma (arrows) and surrounding areas containing aberrant crypts (arrowheads). Insets show cells with high-grade dysplasia lining the adenomatous glands.

(MPM total magnifications: A, E, I, M = 48X, C, G, K, O = 300X, insets = 750X. H&E total magnifications: B, F, J, N = 40X, D, H, L, P = 200X, insets = 400X).

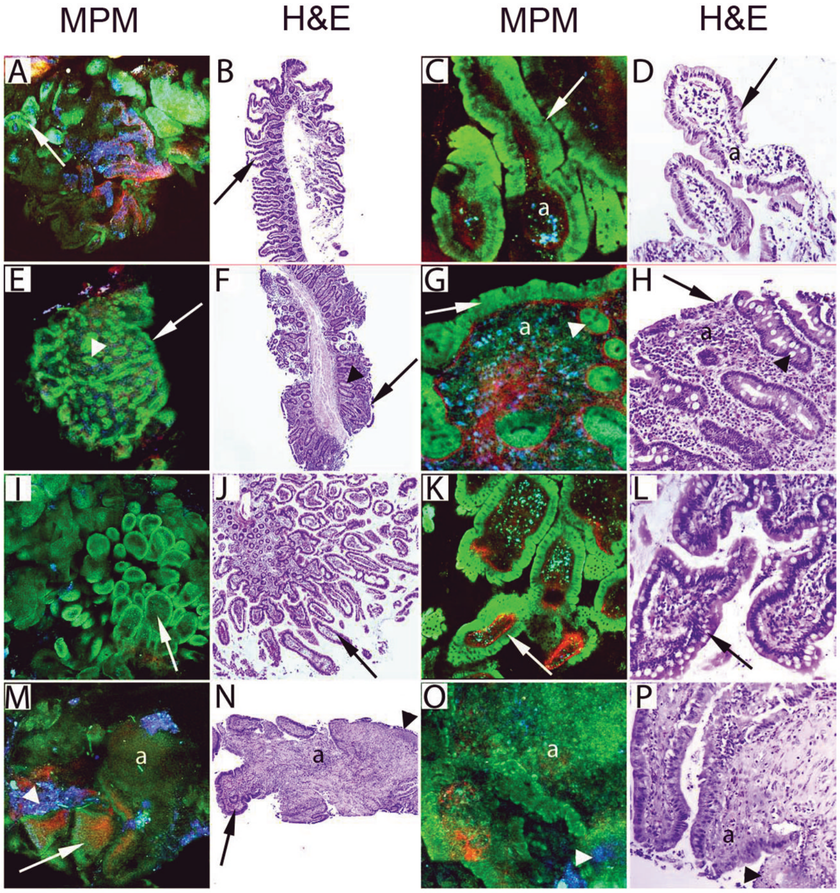

Figure 4.

Imaging of small intestinal lesions from human subjects by MPM and H&E. A–B, Images of the normal duodenum from a control subject show villi (arrows) lining the mucosal surface at low magnification. C–D, High magnification images of panels A and B show enterocytes (green in MPM) and scattered goblet cells (arrows) lining the villi. The core of the villus (a) shows mononuclear cells (mixture of blue and green cells in MPM), recognized mainly as lymphocytes by H&E. E–F, Duodenal biopsy from a subject clinically diagnosed with celiac sprue shows flattened mucosal surface with villus shortening (arrows) and preserved crypts (arrowheads). G–H, High magnification images of panels E and F show the flattened mucosal surface lined by simple columnar cells (arrows) and crypts with goblet cells (arrowheads). The lamina propria (a) has increased inflammatory cell infiltrate (mixture of blue and green cells in MPM), mainly identified as lymphocytes, plasma cells and eosinophils by H&E. I–L, The normal terminal ileum from a control subject shows villi (arrows) at low (I–J) and high (K–L) magnifications. M–P, Ileal biopsy from a subject with Crohn's disease shows morphological features of chronic active ileitis. Low magnification images (M–N) show blunted villi (arrows), focal ulcerations (arrowheads) and inflammatory infiltrate (a). High magnification images (O–P) show focal ulcerations (arrowheads) and inflammatory infiltrate (a) (identified as neutrophils and lymphocytes by H&E).
(MPM total magnifications: A, E, I, M = 48X; C, G, K, O = 300X. H&E total magnifications: B, F, J, N = 40X ; D, H, L, P = 200X)

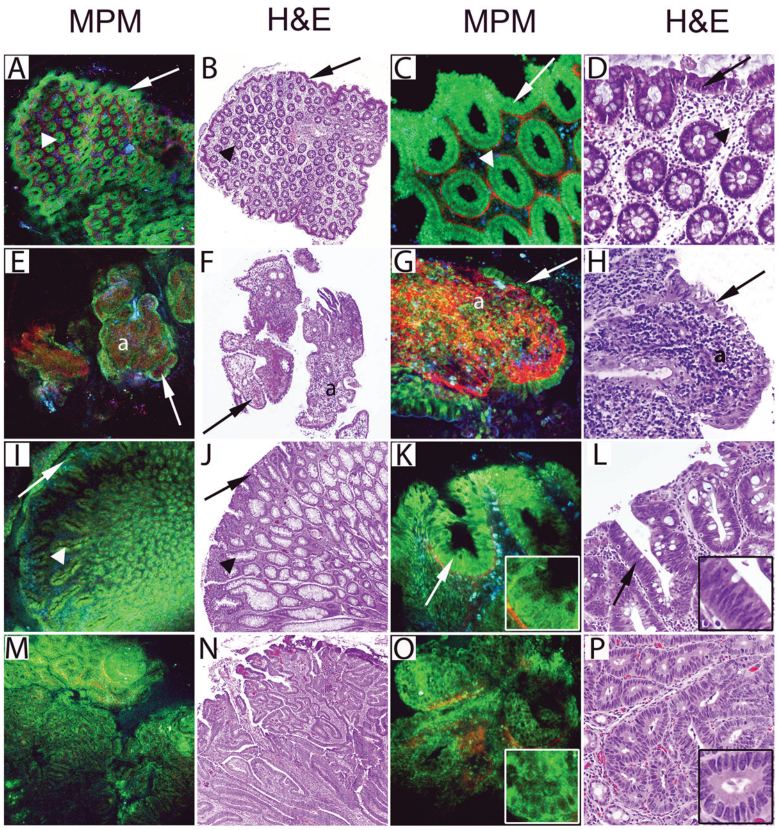

Figure 5.

Imaging of colonic lesions from human subjects by MPM and H&E. A–D, Image of normal colonic mucosa from a control subject shows low (A–B) and high (C–D) magnification images of the surface epithelium (arrows) and crypts (arrowheads) with mononuclear cells in the lamina propria recognized mainly as lymphocytes by H&E. E–H, Distal colonic biopsy from a subject with ulcerative colitis shows morphological features of chronic active colitis. Low magnification images (E–F) show irregular mucosal surface due to ulceration/ pseudopolyps (arrows), reduced numbers of crypts and increased cellularity in the lamina propria (a). The high magnification images (G–H) show a pseudopolyp lined by columnar epithelium (arrow) with complete loss of crypts and marked mononuclear inflammatory cell infiltrate in the lamina propria (a), identified as lymphocytes and plasma cells on H&E. I–L, Images from a tubular adenoma show a smooth polypoid surface (arrows) with adenomatous glands (arrowheads) at low magnification in panels I–J and high magnification images in panels K–L show an adenomatous gland with low-grade dysplasia (arrows and insets). M-P, A well-differentiated adenocarcinoma of the colon is shown at low magnification in panels M–N with complex (back-to-back) glandular arrangement and shown at high magnification in panels O–P revealing crowded glands lined by dysplastic cells (insets).
(MPM total magnifications: A, E, I, M = 48X; C, G, K, O = 300X. H&E total magnifications: B, F, J, N = 40X, D, H, L, P = 200X).

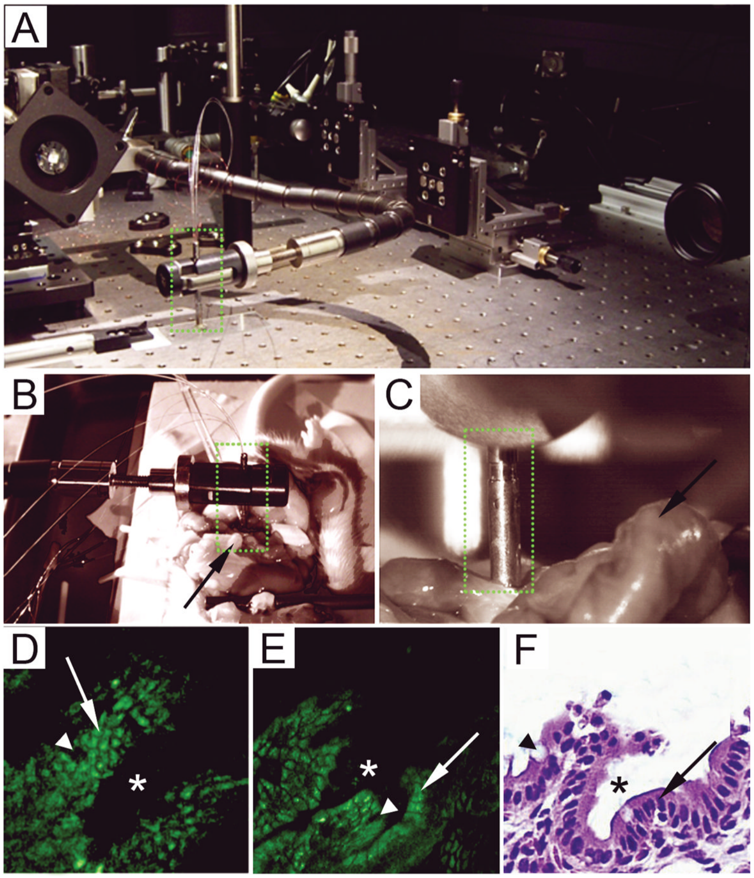

Figure 6.

In vivo MPM imaging using a miniaturized endoscope. A, Photograph of the flexible multiphoton endoscope (green dotted rectangle) used in this study on an optical table, held by an articulating arm. B–C, Infrared CCD camera images of the endoscope while imaging the surgically exposed colonic mucosa of a live, anesthetized rat, at 2x (B) and 10x(C) magnifications. The endoscope is outlined by green dotted rectangles and the rat colon is indicated by the arrows. D, Image of the colonic mucosa of a living rat generated with the flexible MPM endoscope shown in A–C. This unaveraged single image frame shows a field of view of 1153m X 1153m was acquired at 4.1 frames/sec using 75 mW incident power at 800 nm. E, Image of an *ex vivo* section of rat colon, acquired using the bench-top Olympus MPM system at identical dimensions and a comparable focal depth as the endoscope. F, H&E-stained section of the same colon imaged by MPM in panel E. Colonic crypts indicated by "*", enterocytes indicated by arrows and goblet cells indicated by arrowheads.